

## Increased MRI-derived parenchymal cerebral spinal fluid mapping in untreated obstructive sleep apnea patients<sup>☆</sup>

Samantha A. Keil <sup>a</sup>, Yi Li <sup>a</sup>, Ana C. Krieger <sup>b,c,d,e</sup>, Xiuyuan H. Wang <sup>a</sup>, Thanh D. Nguyen <sup>f</sup>, Jana Ivanidze <sup>a,g</sup>, Gloria C. Chiang <sup>a,b</sup>, Tracy A. Butler <sup>a,\*</sup>, Liangdong Zhou <sup>a,\*</sup>

<sup>a</sup> Department of Radiology, Brain Health Imaging Institute (BHII), Weill Cornell Medical College, New York, NY 10065, USA

<sup>b</sup> Weill Cornell Medicine/New York-Presbyterian Hospital, Weill Cornell Medical College, New York, NY 10065, USA

<sup>c</sup> Department of Medicine, Weill Cornell Medical College, New York, NY 10065, USA

<sup>d</sup> Department of Neurology, Weill Cornell Medical College, New York, NY 10065, USA

<sup>e</sup> Department of Genetic Medicine, Weill Cornell Medical College, New York, NY 10065, USA

<sup>f</sup> Department of Radiology, MRI Research Institute (MRIRI), Weill Cornell Medical College, New York, NY 10065, USA

<sup>g</sup> Department of Radiology, Neuroradiology Division, Weill Cornell Medical College, New York, NY 10065, USA

### ARTICLE INFO

#### Keywords:

Obstructive sleep apnea  
Glymphatic fluid  
Parenchymal cerebrospinal fluid  
beta-amyloid  
MRI  
Cognitive function

### ABSTRACT

**Background:** Obstructive sleep apnea (OSA) is a highly prevalent disorder associated with increased risk of Alzheimer's disease (AD) and cognitive decline. The mechanisms underlying the relationship between OSA and disease progression remain undefined, but may involve impairment in the glymphatic system, a perivascular network responsible for cerebrospinal fluid and interstitial fluid exchange and waste clearance. This study evaluated MRI-visible perivascular spaces (PVS) and parenchymal CSF mapping (pCSF) as non-invasive proxies of glymphatic function in untreated and CPAP-treated OSA relative to healthy controls.

**Methods:** Forty-two adults ( $n = 16$  healthy controls,  $n = 14$  untreated OSA,  $n = 12$  CPAP-treated OSA) were retrospectively evaluated. Participants underwent MRI and cognitive testing, and a sub-cohort ( $n = 25$ ) received <sup>11</sup>C-PIB amyloid PET. Enhanced PVS contrast (EPC) mapping segmentation quantified MRI-visible PVS, while multi-echo FAST-T2 MR derived pCSF mapping provided voxelwise quantification of glymphatic fluid distribution. Between-group differences were assessed using nonparametric statistics and multivariable regression analyses controlled for age and sex.

**Results:** Segmented MR-visible PVS did not differ between groups. Comparatively, untreated OSA subjects had higher ADmask pCSF versus than controls ( $p = 0.0155$ ), with exploratory analyses displaying a similar relationship across regions including cerebral grey and white matter. Intriguingly, CPAP-treated individuals exhibited pCSF levels statistically comparable to controls. In the sub-cohort, higher ADmask pCSF independently predicted greater amyloid burden on PET ( $\beta = 0.616$ ,  $p = 0.007$ ).

**Conclusions:** Untreated OSA is associated with higher parenchymal glymphatic fluid burden consistent with impaired perivascular fluid dynamics. CPAP-treated participants exhibited pCSF levels comparable to controls. pCSF mapping represents a sensitive biomarker for evaluating perivascular fluid distribution, a positive association with amyloid deposition, and monitoring potential treatment-related differences in OSA.

### 1. Introduction

Obstructive sleep apnea (OSA) is one of the most prevalent sleep disorders impacting nearly one billion adults globally (Benjafield et al., 2019). Characterized by recurrent episodes of upper airway obstruction during sleep, OSA causes breathing irregularities, drops in oxygen

saturation levels, shortened sleep duration, and cortical arousals fragmenting sleep architecture (Benjafield et al., 2019; Slowik et al., 2025; Chang et al., 2023). When left untreated, OSA patients experience daytime sleepiness and fatigue, impaired cognition, and an increased risk of cardiovascular, metabolic, and neurodegenerative diseases (Benjafield et al., 2019; Slowik et al., 2025; Chang et al., 2023; Bangash

<sup>☆</sup> This article is part of a Special issue entitled: 'Circadian and Sleep Rhythm Disruption' published in Neurobiology of Disease.

\* Corresponding authors at: Brain Health Imaging Institute, 407 E 61<sup>st</sup> St, New York, NY 10065, USA

E-mail addresses: [tab2006@med.cornell.edu](mailto:tab2006@med.cornell.edu) (T.A. Butler), [liz2018@med.cornell.edu](mailto:liz2018@med.cornell.edu) (L. Zhou).

et al., 2020; Kim, 2012). Although epidemiological studies implicate OSA and other sleep disorders as primary risk factors in Alzheimer's disease (AD) and related dementias (Ungvari et al., 2025; Gribsholt et al., 2025), the mechanisms by which sleep-disordered breathing accelerates neurodegenerative progression remain poorly understood.

Over the last decade, impairment in the brain's waste clearance system, or glymphatic system (Iliff et al., 2012), has been implicated in neuropathologic disease progression in AD preclinical models (Iliff et al., 2012; Xie et al., 2013; Harrison et al., 2020; Ishida et al., 2022; Pedersen et al., 2023; Simon et al., 2022; Xu et al., 2015; Keil et al., 2025). Utilizing a perivascular network for cerebrospinal fluid (CSF) and interstitial fluid (ISF) exchange, effective glymphatic clearance relies on perivascular aquaporin-4 localization (Iliff et al., 2012; Pedersen et al., 2023; Simon et al., 2022; Mestre et al., 2018a) and vascular pulsatility (Iliff et al., 2013; Mestre et al., 2018b; van Veluw et al., 2020). Shown to be predominantly sleep-active (Xie et al., 2013; Hablitz et al., 2020), it is further regulated by circadian rhythm (Hablitz et al., 2020) and central noradrenergic tone (Hablitz et al., 2019; Benveniste et al., 2017) and closely coupled to synchronous low-frequency neural activity (Jiang-Xie et al., 2024). In animals, sleep disruption impairs glymphatic clearance (Kang et al., 2009; Holth et al., 2019), and glymphatic impairment has been directly associated with increased cortical amyloid-beta (Iliff et al., 2012; Pedersen et al., 2023; Simon et al., 2022; Xu et al., 2015; Mestre et al., 2018a), tau (Harrison et al., 2020; Ishida et al., 2022; Iliff et al., 2014), and a-synuclein (Lopes et al., 2025; Cui et al., 2021) deposition. In humans, several gadolinium enhanced neuroimaging studies support these findings, with increased EEG delta and reduced beta power and heart rate being associated with glymphatic influx and clearance rates (Dagum et al., 2025), and acute experimental sleep deprivation with slower clearance (Dagum et al., 2025; Eide et al., 2021). Taken together, we might expect that patients with OSA, who experience intermittent hypoxemia, alterations in vascular pulsatility, and loss of sleep continuity, might be particularly susceptible to glymphatic impairment and subsequent neuropathologic disease progression.

While these contrast-based neuroimaging studies show promise, broad clinical assessment of glymphatic impairment requires non-invasive, reproducible and broadly applicable techniques (Keil et al., 2025). While assessments of MRI-visible enlarged perivascular space (PVS) burden has been used as an indirect marker of glymphatic stasis and dysfunction (Sepehrband et al., 2019), this approach suffers from notable limitations in sensitivity and specificity (Keil et al., 2025; Zhou et al., 2025).

Parenchymal CSF (pCSF) mapping via multi-echo FAST-T2 MRI provides a novel, non-invasive, and clinically feasible voxel-wise estimate of long-T2 water (200–2000 ms) comparable to CSF within other CSF spaces and thought to reflect perivascular "glymphatic fluid" throughout the parenchyma PVS (Zhou et al., 2025; Zhou et al., 2023; Zhou et al., 2024a). Importantly this is differentiated from short-T2 associated myelin water (0–20 ms) and intermediate-T2 corresponding intra/extracellular water inclusive of interstitial fluid (20–200 ms). Thereby, this approach expands perivascular CSF assessment from MRI-visible PVS in white matter (WM) to additionally include PVS in cerebral cortical grey matter PVS that is sub-voxel and invisible at typical MRI resolution. Prior studies demonstrate that pCSF is positively associated with normal aging (Zhou et al., 2023) and amyloid burden (Zhou et al., 2024a) and correlates more strongly with regional amyloid PET than PVS quantified traditionally in white matter or using diffusion-derived free water (DTI-FW) approaches (Zhou et al., 2025).

In this study, we assessed two MRI-derived markers of perivascular fluid distributions including the traditional white-matter visible enlarged PVS volume and the novel pCSF mapping, in subjects with either untreated OSA or continuous positive airway pressure (CPAP)-treated OSA, against cognitively normal healthy controls (HC). The primary objective was to characterize differences in perivascular fluid distribution across these cohorts, with exploratory examination of associations between pCSF across measures of OSA severity, as well as

regional PET-defined amyloid in a subset of participants. In consideration of the association between sleep disruption and altered brain fluid clearance dynamics (Xie et al., 2013; Dagum et al., 2025; Eide et al., 2021), we hypothesized that participants with untreated OSA would display elevated perivascular fluid levels defined by both PVS and pCSF. Further we hypothesized that greater pCSF burden would be associated with both increased OSA severity at baseline and increased amyloid burden on PET.

By defining patterns of perivascular fluid distribution associated with OSA associated sleep disruption, this work aims to define the potential utility of non-invasive neuroimaging biomarkers in characterizing perivascular glymphatic fluid alterations relevant to sleep disruption and neurodegenerative disease risk.

## 2. Methods

### 2.1. Ethics approval

#### 2.1.1. Consent to participate and publish

The neuroimaging and cognitive assessments evaluated within this study were approved by the Institutional Review Board and written and informed consent for data use and publication was obtained from all participants.

### 2.2. Participants

In this cross-sectional study (Fig. 1), 42 subjects were retrospectively identified from within the Brain Health Imaging Institute (BHII) repository and were classified as either untreated OSA ( $n = 14$ ), CPAP-treated OSA ( $n = 12$ ), or age- and sex- matched healthy controls (HC;  $n = 16$ ) (Table 1).

OSA diagnosis and treatment status across individuals was established through clinical documentation within BHII. Initial diagnosis relied on either polysomnography or home sleep testing using the combined apnea-hypopnea index (AHI) and 4% oxygen desaturation criteria. CPAP-treated individuals were categorized after clinical documentation of at least 6-months of treatment prior to imaging. Within this cohort, baseline OSA severity was evaluated in metrics of apnea-hypopnea index (AHI), minimum oxygen saturation (SaO (Slowik et al., 2025)), and standard categorical AHI thresholds (5–14 = mild; 15–29 = moderate; 30+ = severe). For a subset of participants (untreated  $n = 1$ , treated  $n = 2$ ), formal polysomnography was performed at an external clinical site, and baseline severity metrics were unavailable.

All subjects underwent standardized evaluations for cognitive performance by a cognitive neurologist, MRI, and in a subset of participants  $^{11}\text{C}$ -PiB PET ( $n = 25$ ). MRI and PET examinations were reviewed by a board-certified radiologist with more than 15 years of experience, and all subjects were reviewed for final diagnosis in a multidisciplinary consensus conference.

### 2.3. Cognitive testing and sleep quality assessment

All subjects underwent standardized cognitive evaluations by a Clinical Neuropsychologist consisting of clinical and neurological exams including the Clinical Dementia Rating Scale (CDR) (Morris, 1997) and Montreal Cognitive Assessment – Blind version (MoCA; 22 Blind) (Lord et al., 2024). Global CDR scores range from 0 to 3 with 0 considered cognitively unimpaired while a CDR  $\geq 0.5$  indicative of cognitive impairment. For the MoCA-Blind which ranges from 0 to 22, scores  $<18$  are suggestive of cognitive impairment. For each BHII participant, a multidisciplinary consensus conference including neurology, radiology, and neuropsychology was used to clinically diagnose each participant as either cognitively normal or impaired (mild cognitive impairment (MCI) or dementia). Cognitive status was not an exclusion criterion for assessment in this study.

Global sleep quality was evaluated across groups using the validated

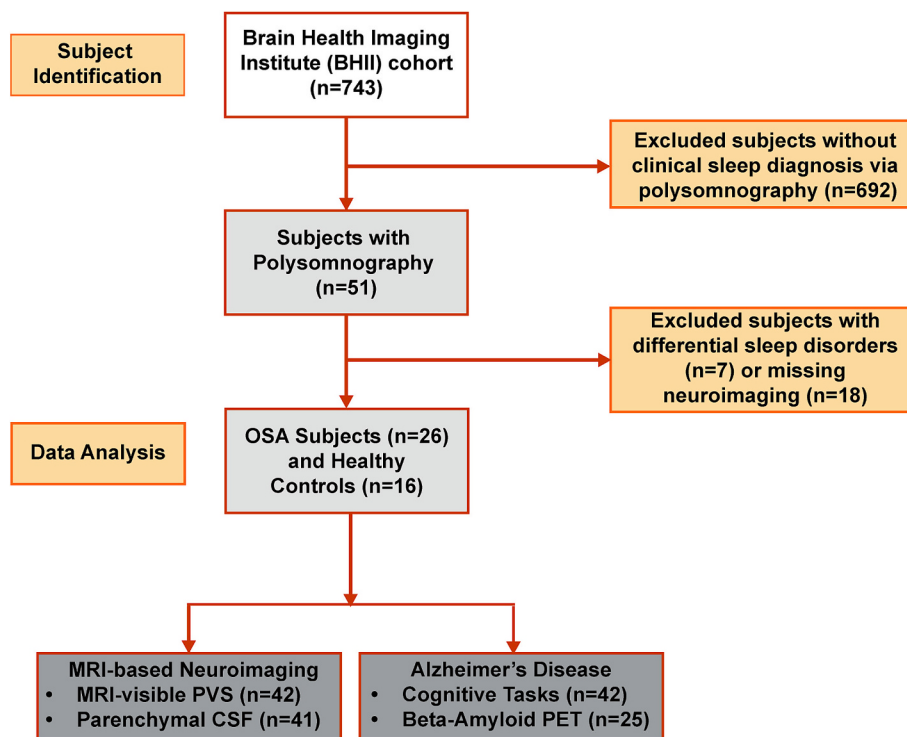


**Fig. 1.** Strobe Diagram. Flow diagram of participant identification, exclusions, and final analytic cohorts derived from the BHII repository. Of 743 BHII participants, 51 had available clinical sleep diagnosis. Participants with alternative sleep diagnoses ( $n = 7$ ) or neuroimaging ( $n = 18$ ) were excluded. Final analytic samples are as noted, with differences in sample size reflecting modality-specific data availability.

Pittsburgh Sleep Quality Index (PSQI) (Buysse et al., 1989). The PSQI assesses individual domains of subjectively reported sleep quality, latency, duration, efficiency, disturbance, medication use, and daytime dysfunction. With total score ranging from 0 to 21, poor sleep quality is defined by any score  $> 5$ .

#### 2.4. MRI imaging acquisition

All MRIs were acquired on a Siemens Prisma 3 T scanner using a 64-channel head-neck coil with neuroimaging sequences consisting of 3D T1W from MPRAGE for ROI parcellation and T2W from T2-SPACE for MR-visible PVS assessment, a T2 FLAIR for white matter hyperintensity (WMH) delineation, and a multi-echo 3D spiral FAST-T2 sequence for pCSF mapping (Zhou et al., 2023). These were acquired with the following parameters: 1) 3D sagittal T1W MPRAGE: TR/ TE/TI = 2300/ 2.3/900 ms, flip angle =  $8^\circ$ , readout bandwidth (rBW) = 200 Hz/pixel, voxel size = 1.0 mm isotropic, GRAPPA parallel imaging factor (R) = 2, scan time = 5.5 min; 2) 3D sagittal T2W SPACE: TR/TE = 3200/408 ms, flip angle =  $90^\circ$ , rBW = 751 Hz/pixel, turbo factor = 285, voxel size = 1.0 mm isotropic, scan time = 5 min; 3) 3D sagittal T2 FLAIR with fat saturation: TR/TE/TI = 4000/384/2400 ms, echo spacing = 3.46 ms, flip angle =  $90^\circ$ , rBW = 751 Hz/pixel, turbo factor = 278, voxel size = 1.0 mm isotropic, R = 2, scan time = 5.4 min; 4) 3D multi-echo FAST-T2 sequence (Zhou et al., 2023): spiral TR/TE = 7.8/0.5 ms, six echo times = 0 (T2-prep turned off), 7.5, 17.5, 67.5, 147.5 and 307.5 ms, flip angle =  $10^\circ$ , rBW = 1042 Hz/pixel, number of slices per slab = 80, number of spiral leaves collected per T2prep = 64, voxel size =  $1.3 \times 1.3 \times 2 \text{ mm}^3$ , scan time = 7 min.

#### 2.5. PET imaging acquisition

A subset of subjects ( $n = 25$ ) received  $^{11}\text{C}$ -PiB amyloid-beta (A $\beta$ ) PET imaging using the Siemens Biograph mCT-S (64) slice PET/CT, according to previously published acquisition protocol (Zhou et al., 2025; Zhou

et al., 2024a). All data was acquired in 3D list mode from 40 to 90 min after rapid bolus injection of  $\sim 555$  MBq. PiB PET images were reconstructed to a  $512 \times 512 \times 74$  matrix of  $0.8 \times 0.8 \times 3$  mm voxels in  $5 \times 10$  frames from 50 to 70 min.

#### 2.6. Image processing

##### 2.6.1. MRI region of interest parcellation

Each T1W MRI was segmented using FreeSurfer (Fischl, 2012) version 7.1 *recon-all* command for region of interest (ROI) parcellation. The white matter hyperintensity mask was excluded from white matter volume to minimize its effect on enlarged PVS segmentation and pCSF mapping. Analysis of MRI-visible PVS, pCSF, and PiB were described below. ROIs used for extracting values of pCSF and PiB measured amyloid burden were eroded by 1-voxel to reduce the partial volume effect (PVE).

##### 2.6.2. MR-visible PVS

Segmentation of enlarged MR-visible PVS in white matter was performed using a deep learning-based model, with a weakly supervised approach via Frangi filter segmented PVS<sup>39</sup>. Under this approach, the T1W was registered to the T2W space, and an enhanced PVS contrast (EPC) map is derived from the T1W to T2W ratio (Sepehrband et al., 2019; Lan et al., 2023). Subject to this approach, PVS segmentation on EPC is constrained to the Freesurfer defined WM ROI. After excluding WMH from the EPC PVS mask (Li et al., 2024), the total enlarged PVS volume is normalized by the WM volume to obtain the PVS/WMV ratio.

##### 2.6.3. pCSF mapping

Parenchymal CSF (pCSF) maps were obtained using non-linear least square fitting of three-exponential T2 models with L2 regularization, consistent with previous reports (Zhou et al., 2025; Zhou et al., 2023; Zhou et al., 2024a; Nguyen et al., 2016). This approach decomposes voxel-wise water signal into short-T2 myelin water (T2: 0–20 ms),

**Table 1**

Demographic Table. Abbreviations: Apnea-hypopnea Index (AHI); Apolipoprotein E4 allele (APOE4); Blood Pressure (BP); Body Mass Index (BMI); Clinical Dementia Rating Scale (CDR); Healthy Control (HC); Minimum (Min); Montreal Cognitive Assessment (MoCA); Obstructive Sleep Apnea (OSA); Oxygen Saturation ( $\text{SaO}_2$ ); Pittsburgh Sleep Quality Index (PSQI); Standard Deviation (SD). Baseline OSA metrics were unavailable for  $n = 1$  untreated and  $n = 2$  CPAP-treated participants due to external sleep evaluation, and analyses involving these metrics was performed on available data only.

	Healthy Controls ( $n = 16$ )	Untreated OSA ( $n = 14$ )	Treated OSA ( $n = 12$ )	Statistical Test	<i>p</i> -value
Age, mean (SD)	67.2 (7.2)	69.9 (11.5)	65.6 (8.9)	Kruskal-Wallis	0.543
Female/Male	6/10	7/7	3/9	Chi-Squared	0.424
Ethnicity (%)				Chi-Squared	0.477
White (non-Hispanic)	15 (93.7)	11 (78.6)	10 (83.3)		
Other	1 (6.3)	3 (21.4)	2 (16.7)		
Education (SD)	16.1 (2.3)	17.1 (1.9)	16.5 (2.9)	Kruskal-Wallis	0.538
APOE4 Carrier (%)	4 (25)	2 (14.3)	4 (33.3)	Chi-Squared	0.519
BMI (SD)	25.4 (2.9)	25.4 (4.9)	30.2 (5.9)	Kruskal-Wallis	0.056
Systolic BP (SD)	130.9 (18.5)	127.8 (10.9)	128.8 (11.9)	Kruskal-Wallis	0.758
Diastolic BP (SD)	78.6 (9.7)	75.0 (11.1)	74.4 (8.4)	Kruskal-Wallis	0.368
Global CDR (SD)	0 (0)	0.42 (0.3)	0.3 (0.26)	Kruskal-Wallis	<0.001
MOCA (SD)	20.46 (0.7)	16.9 (4.2)	17.8 (2.1)	Kruskal-Wallis	0.002
Cognitive Impairment (%)	0 (0)	8 (57.1)	5 (41.7)	Fisher's Exact	<0.001
Global PSQI (SD)	4.83 (2.5)	7.55 (3.9)	5.46 (2.8)	Kruskal-Wallis	0.222
Baseline AHI (SD)		13.3 (10.7)	27.1 (32.1)	Mann-Whitney	0.365
Baseline Min $\text{SaO}_2$ (SD)		83.2 (3.8)	84.8 (2.2)	Mann-Whitney	0.344
Baseline OSA Severity (%)				Chi-Squared	0.009
Mild (AHI 5–14)		12 (85.7)	3 (25)		
Moderate (AHI 15–29)		0 (0)	4 (33.3)		
Severe (AHI 30+)		2 (13.3)	3 (25)		

intermediate-T2 intra/extracellular water containing interstitial fluid and intracellular fluid (T2: 20–200 ms), and long-T2 perivascular CSF-like water (T2: 200–2000 ms). We operationally define pCSF as the long-T2 fraction within brain parenchyma's perivascular spaces ("glymphatic fluid"). This water is freely movable and characteristically comparable to CSF in other CSF spaces. Upon delineation, pCSF were rigidly co-registered to FreeSurfer T1W space using normalized mutual information criteria.

Regional pCSF was also calculated within a composite ROI consisting of regions susceptible to amyloid deposition, termed ADmask (Zhou et al., 2025; Zhou et al., 2024a; Mosconi et al., 2010; Zhou et al., 2024b). The ADmask, defined within each participant's native T1W space using FreeSurfer parcellation is a meta-ROI encompassing AD-vulnerable cortical regions including inferior parietal, inferior/middle/superior temporal, caudal/rostral middle frontal, posterior cingulate, and precuneus. It was defined and used in previous work within our group linking early amyloid deposition and neurodegenerative decline (Lin et al., 2024; Wang et al., 2023) as well as pCSF-amyloid associations

(Zhou et al., 2025; Zhou et al., 2024a). Given the established relevance of AD-vulnerable cortex to OSA-related neurodegenerative risk, ADmask was specified a priori as the primary ROI for hypothesis-driven analyses.

#### 2.6.4. PET imaging processing

The dynamic frames of PiB PET from 50 to 70 min (4 frames  $\times$  5 min/frame) were realigned and summed, and the summed image was then coregistered to the individual FreeSurfer T1W space using the normalized mutual information method in FSL. Then the  $^{11}\text{C}$ -PiB standard uptake value ratio (SUVR) was calculated by normalizing the whole brain voxelwise standard uptake value (SUV) with that in the cerebellar cortex (Zhou et al., 2025; Zhou et al., 2024a; Villemagne et al., 2013). Enabling direct comparison with pCSF analyses. PiB A $\beta$  SUVR quantification was evaluated within the ADmask region (Zhou et al., 2025; Zhou et al., 2024a; Mosconi et al., 2010; Zhou et al., 2024b). The average ADmask SUVR served as the overall measure of A $\beta$  deposition across subjects.

#### 2.7. Statistical analysis

Statistical analyses were performed in RStudio (Version 4.4.2; R Foundation for Statistical Computing) and GraphPad Prism (Version 10.1; GraphPad Software, San Diego, CA). Given the small and variable subject size across groups ( $n = 10$ –16), non-parametric models were prioritized for analyses. Between-group comparisons of demographic and clinical variables were analyzed using Kruskal-Wallis test followed by Dunn's post hoc comparisons. Categorical variables were analyzed using  $\chi^2$  tests. For variables collected only in OSA participants, Mann-Whitney tests were used to compare untreated and CPAP-treated groups. Multivariable linear regression models were used to assess the independent effects of OSA status (untreated, treated and healthy controls), with age and sex as covariates. Moreover, the relationship between pCSF and PET-measured amyloid burden was investigated by controlling for age, sex, as well as diagnoses. Leave-one-out testing approach was utilized to avoid the potential overfitting effect. Model performance was evaluated with F-statistics. All tests were two-tailed, with  $p < 0.05$  considered statistically significant.

### 3. Results

#### 3.1. Demographics

Demographic characteristics of the study population are summarized in Table 1. Groups did not differ in age, sex, ethnicity, or education. Similarly, APOE4 status, body mass index, and blood pressure were balanced.

There was a significant overall difference across groups for CDR (Kruskal-Wallis H (2) = 16.56,  $p = 0.0003$ ), with both untreated ( $p = 0.0004$ ) and CPAP-treated participants ( $p = 0.0141$ ) having higher average CDR compared to healthy controls, with some participants reaching threshold for impairment. Similarly, MoCA-Blind scores differed significantly across groups (Kruskal-Wallis H(2) = 12.79,  $p = 0.0017$ ), with both untreated ( $p = 0.0046$ ) and CPAP-treated OSA participants ( $p = 0.0083$ ) demonstrating mean scores below the threshold suggestive for cognitive impairment (<18), compared to healthy controls which remain above. Consistent with these continuous measures, the portion of participants classified as cognitively impaired (MCI/dementia) differed significantly across groups (Fisher's exact test,  $p = 0.0008$ ), with impairment exclusively observed in OSA groups.

To assess the individual contributors of cognitive performance, multivariable linear regression adjusting for age, sex and OSA status demonstrated a significant overall model ( $F(4,33) = 4.07, p = 0.0087$ ). Relative to healthy controls, both untreated ( $\beta = -3.88, \text{CI}_{95\%} -6.07$  to 1.68,  $p = 0.0011$ ) and CPAP-treated participants ( $\beta = -2.639, \text{CI}_{95\%} -4.95$  to  $-0.33, p = 0.0264$ ) are independently associated with lower MoCA-Blind scores. Together, these results support previous findings

that OSA is associated with reduced cognitive performance (Chang et al., 2023).

### 3.2. Sleep demographics

Global self-reported sleep quality, as measured by PSQI, did not differ significantly across groups, with mean scores of  $4.83 \pm 2.5$  in healthy controls,  $7.55 \pm 3.9$  in untreated OSA, and  $5.46 \pm 2.6$  in CPAP-treated OSA. However, a PSQI score greater than 5, consistent with the validated threshold for poor sleep quality, was observed in both untreated and CPAP-treated participants, while controls remain below. While there was no difference in AHI or minimum SaO (Slowik et al., 2025) across OSA participants with baseline OSA severity ( $n = 23$ ), there was a significant difference in categorical distribution ( $p = 0.0092$ ) across groups. This is likely due to treatment recommendation after evaluation of OSA severity clinically.

We evaluated whether pCSF is associated with baseline metrics of OSA severity through scatter plots and simple linear regression (Supplementary Fig. S1). No significant associations were observed across all OSA subjects and when analyses were stratified by treatment status (all  $p > 0.1$ ). Together, this suggests that pCSF differences are not explained by severity metrics alone.

### 3.3. MRI-visible PVS

The volume of visible PVS in WM quantified using enhanced PVS contrast (EPC) mapping (Sepehrband et al., 2019), did not differ (Fig. 2) across groups (Kruskal-Wallis  $H(2) = 0.8053$ ,  $p = 0.6686$ ), with a range of 1.38–1.59% global WM quantified as enlarged PVS. While the representative compressed three-dimensional EPC renderings (Fig. 2A bottom) reflect potential variance in continuity and morphology of the white matter visible PVS, these qualitative differences do not translate to statistically significant group-level differences after quantitative normalization by white matter volume. White matter normalization, standard across volumetric assessments, accounts for inter-individual variability caused by either brain size or neurodegenerative atrophy. Importantly, white matter volume did not significantly differ across groups (Kruskal-Wallis  $H(2) = 5.032$ ,  $p = 0.081$ ; Supplementary Table S2).

### 3.4. pCSF burden

In contrast, pCSF (Zhou et al., 2025; Zhou et al., 2023; Zhou et al., 2024a) mapping revealed robust group differences across multiple regions, as detailed in Supplementary Table S1. Fig. 3A shows the representative pCSF maps for subjects in three diagnostic groups. Within the global ADmask ROI (Mosconi et al., 2010) (Kruskal-Wallis  $H(2) = 7.868$ ,  $p = 0.0196$ ), untreated OSA participants exhibited significantly higher pCSF compared to healthy controls ( $p = 0.0155$ ), while CPAP-treated individuals did not differ from either group (Fig. 3B). No significant differences were observed in intracranial volume normalized ADmask volume (Kruskal-Wallis  $H(2) = 0.98$ ,  $p = 0.61$ ; Supplementary Table S2).

A multivariable linear regression analysis adjusting for age and sex demonstrated a significant overall model ( $F(4,37) = 5.75$ ,  $p = 0.0011$ ; adjusted  $R^2 = 0.32$ ) wherein untreated OSA was independently associated with increased pCSF within the ADmask ( $\beta = 0.489$ ,  $CI_{95\%} 0.17$  to  $0.81$ ,  $p = 0.0035$ ) compared to healthy controls. Similarly, age showed a positive association with ADmask pCSF ( $\beta = 0.024$ ,  $CI_{95\%} 0.009$  to  $0.039$ ,  $p = 0.0024$ ), consistent with prior reports of age-related increases in glymphatic fluid burden (Zhou et al., 2023). The inclusion of BMI within this model, addressing its potential confound due to group differences, showed that BMI was not independently associated with ADmask pCSF and did not attenuate the observed association between OSA status or age, indicating group differences were not driven by BMI-related effects.

To compliment the hypothesis-driven ADmask analysis, we also performed exploratory analyses across global and focalized regions of interest (Supplementary Table S1). Cerebral grey matter and white matter pCSF both displayed a significantly higher pCSF in untreated OSA participants compared to healthy controls (Kruskal-Wallis  $H(2) = 8.151$ ,  $p = 0.017$ ;  $p = 0.0181$  and  $H(2) = 7.754$ ,  $p = 0.0207$ ;  $p = 0.0215$ , respectively). Similarly, when evaluated at a lobar scale, untreated OSA participants similarly demonstrated greater pCSF within the frontal lobe (Kruskal-Wallis  $H(2) = 9.885$ ,  $p = 0.0071$ ;  $p = 0.0133$ ), parietal lobe (Kruskal-Wallis  $H(2) = 6.429$ ,  $p = 0.0402$ ;  $p = 0.0337$ ), and temporal lobe (Kruskal-Wallis  $H(2) = 6.2$ ,  $p = 0.045$ ;  $p = 0.0383$ ). A significant group difference was additionally detected between healthy controls and CPAP-treated participants within the frontal lobe ( $p = 0.0408$ ). This relationship was maintained across smaller AD and neurodegenerative

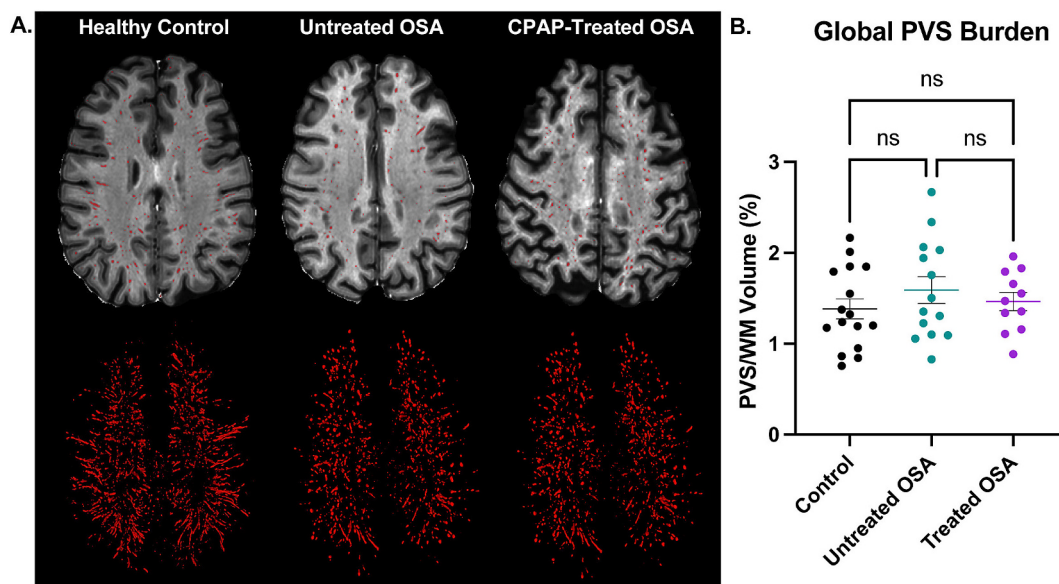


**Fig. 2.** Enhanced Perivascular Space Segmentation shows no significant difference in white matter MRI-visible perivascular spaces between groups. A. Representative images of PVS distributions in Healthy Controls, Untreated OSA, and CPAP Treated OSA subjects with the T1-W and FreeSurfer ROI overlay (top) and 3D rendering (bottom). B. No significant difference in the mean normalized PVS volume (white matter PVS volume/ white matter volume) by Kruskal-Wallis ( $H(2) = 0.8053$ ,  $p = 0.6686$ ).

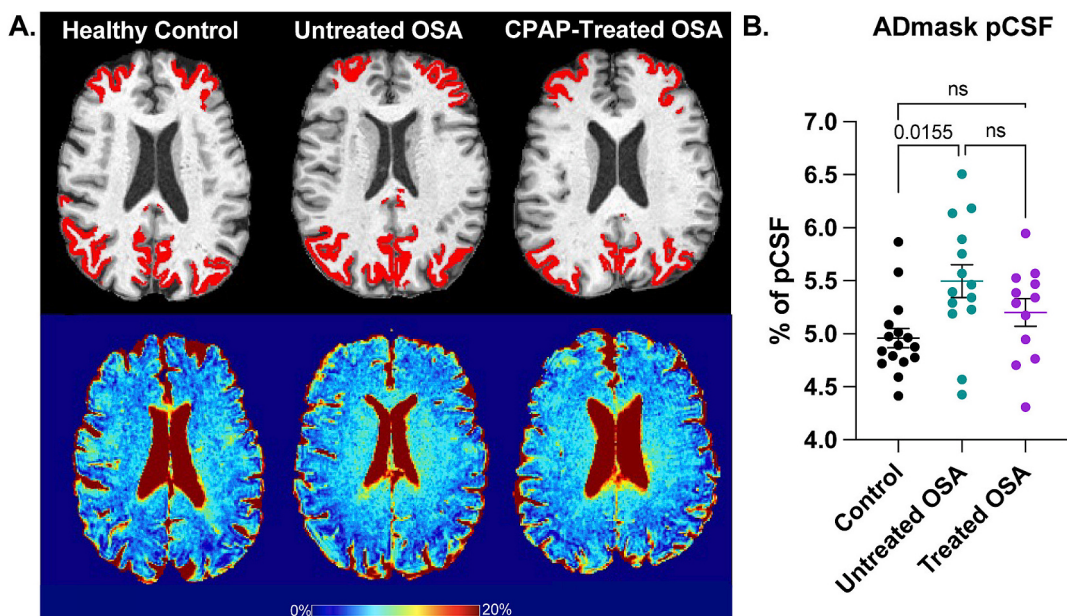


**Fig. 3.** Increased ADmask pCSF in untreated OSA compared to healthy controls. A. ROIs within the ADmask region overlay on each subject's T1W (top) and the corresponding pCSF maps with window size [0, 20%] (bottom). B. pCSF showed a significant group difference (Kruskal-Wallis  $H(2) = 7.868$ ,  $p = 0.0196$ ), with untreated OSA participants exhibiting higher pCSF compared to healthy controls ( $p = 0.0155$ ), and CPAP-treated individuals exhibiting no significant difference from healthy control or untreated OSA participants.

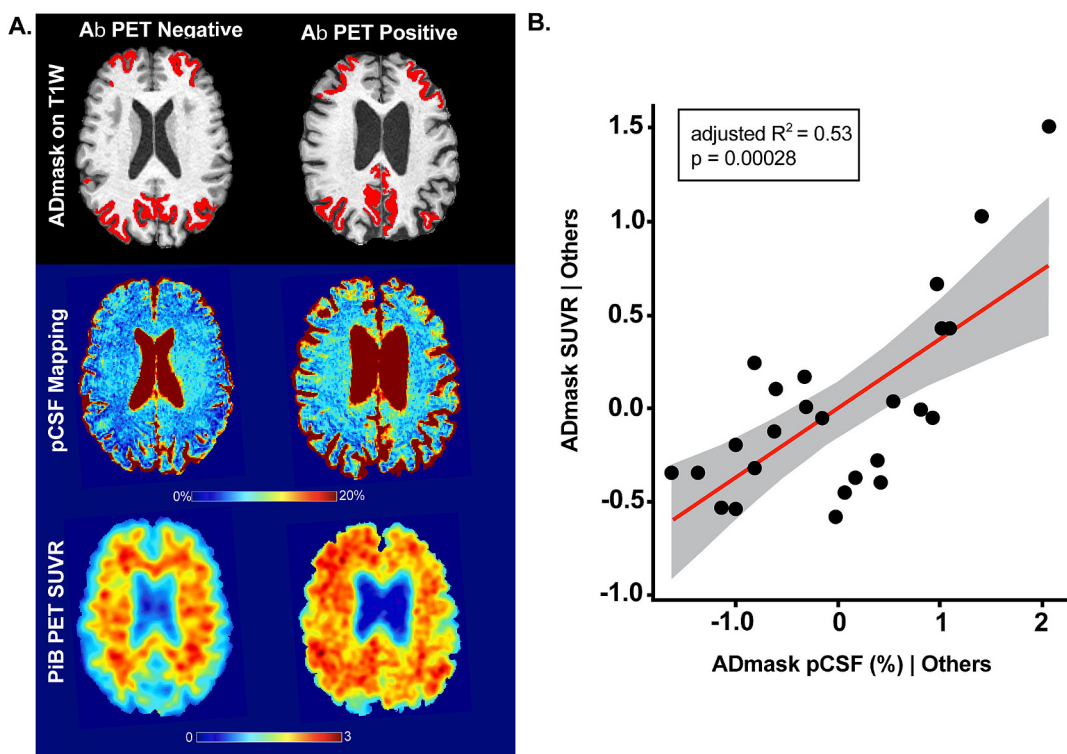


**Fig. 4.** Association between pCSF and amyloid deposition. A. Representative images from both Ab- (left) and Ab+ (right) showing the FreeSurfer-defined ADmask overlaid on native T1 MRI (top), corresponding pCSF maps expressed as percentage (range 0–20%; middle), and PiB-PET SUVR maps (range 0–3; bottom). B. Scatter plot demonstrating the relationship between ADmask pCSF and PiB-PET SUVR across participants with PET imaging ( $n = 25$ ). The red line represents the fitted multivariable linear regression adjusted for age and sex, with the  $CI_{95\%}$  indicated in grey. Higher ADmask pCSF was independently associated with greater amyloid burden ( $\beta = 0.37$ ,  $CI_{95\%} 0.21$ – $0.54$ ,  $p = 0.00018$ ), with the overall model explaining a substantial proportion of the variance (adjusted  $R^2 = 0.53$ ). (For interpretation of the references to colour in this figure legend, the reader is referred to the web version of this article.)

associated regions. Importantly, there was no significant difference observed in regional volumes across groups (Supplementary Table S2), supporting that these pCSF findings are associated with alteration in glymphatic fluid distribution across these regions of interest.

### 3.5. A $\beta$ deposition and pCSF

A subset of participants ( $n = 25$ ; 7 healthy control, 10 untreated, and 8 CPAP-treated) underwent  $^{11}\text{C}$ -PiB PET imaging for the evaluation of amyloid burden. Fig. 4A showed the examples of pCSF mapping and amyloid PET SUVR for amyloid positive and negative participants. Across all participants, multivariable linear regression adjusting for age and sex showed that higher ADmask pCSF was significantly associated with greater A $\beta$  burden ( $\beta = 0.37$ , CI<sub>95%</sub> 0.21 to 0.54,  $p < 0.001$ ). This model explained a substantial proportion of the variance in PiB SUVR (adjusted  $R^2 = 0.53$ ;  $F(3,21) = 9.96$ ,  $p = 0.0003$ ; Fig. 4B). To account for potential over-fitting within this small sub-cohort, a leave-one-out cross-validation analysis was performed. Across iterations, the association between ADmask pCSF and PiB SUVR remained stable, with  $\beta$  values ranging from 0.27 to 0.4 (median  $\beta = 0.37$ ),  $p$ -values consistently  $<0.005$ , and model performance metrics ranging from  $R^2 = 0.43$ –0.6, together indicating that this relationship is not spurious.

Despite this continuous association, there was no observable group-level differences in A $\beta$  burden within the ADmask across diagnostic categories (Kruskal-Wallis H(2) = 0.4484,  $p = 0.80$ ). We next evaluated whether OSA status independently predicted A $\beta$  burden or altered the observed pCSF-PiB SUVR relationship. OSA status did not independently associate with global A $\beta$  burden within this cohort. However, a multi-variable linear regression adjusting for age, sex, and OSA status ( $F(5,19) = 3.32$ ,  $p = 0.02535$ ; adjusted  $R^2 = 0.33$ ) still displayed an independent association of higher ADmask pCSF with increased PiB SUVR ( $\beta = 0.616$ , CI<sub>95%</sub> 0.19 to 1.04,  $p = 0.0069$ ). Collectively, these findings indicate that while pCSF is robustly associated with A $\beta$  deposition, OSA status alone does not account for variability in A $\beta$  burden within this cohort.

## 4. Discussion

This study is the first to demonstrate that untreated OSA is associated with increased MR-derived pCSF mapping, reflecting altered glymphatic fluid distribution, with downstream association to A $\beta$  burden. Across most regions of analysis, participants with untreated OSA exhibited higher pCSF compared to healthy controls, while CPAP-treatment participants displayed pCSF levels comparable to controls. Notably, pCSF did not scale linearly with baseline AHI or minimum SaO (Slowik et al., 2025), suggesting that these imaging differences are not explained by OSA severity metrics alone. Together, these findings expand on prior work associating impaired sleep in OSA to AD risk (Ungvari et al., 2025; Gribsholt et al., 2025) by identifying pCSF burden as a sensitive MRI-derived neuroimaging biomarker at the intersection of sleep disruption and neuropathologic A $\beta$ .

OSA is characterized by recurrent cycles of upper airway obstruction with resultant hypoxemia and sleep fragmentation—factors that collectively disrupt cerebrovascular regulation and perivascular fluid dynamics. Attenuation of arterial pulsatility and disrupted slow-wave activity during apneic events may reduce CSF inflow along periarterial pathways and the interstitial fluid expansion thought to facilitate solute clearance (Xie et al., 2013; Iliff et al., 2013; Mestre et al., 2018b; van Veluw et al., 2020). Similarly, chronic intermittent hypoxia may further promote endothelial dysfunction, oxidative stress, and astrocytic activation, which can alter the aquaporin-4 polarization necessary for glymphatic exchange (Kohler and Stradling, 2010; Kim et al., 2024a). These pathophysiologic processes are hypothesized to impede glymphatic clearance, leading to fluid stasis and enlargement of perivascular spaces, particularly in regions sensitive to vascular compromise. To evaluate whether these theorized glymphatic changes occur in OSA,

herein we comparatively assessed MRI-visible perivascular spaces and parenchymal CSF maps across participants.

### 4.1. Comparison with traditional PVS segmentation

In this cohort, we did not detect significant group differences in MRI-visible PVS using conventional EPC (Sepehrband et al., 2019). Across all groups, EPC volume ranged from 1.3 to 1.6% of total white matter volume, with no measurable elevation in untreated or CPAP-treated OSA participants relative to healthy controls. Our finding contrasts several prior studies using comparable MRI-visible PVS assessments, which report greater PVS burden in OSA, particularly in the basal ganglia and frontal white matter (Jia et al., 2021; Lin et al., 2024; Wang et al., 2023). This is perhaps not surprising, given the larger and clinically more severe OSA cohorts, variation in region-specific quantification compared to our global white matter EPC assessment, and methodological variance in image resolution, segmentation algorithms, and normalization procedures. As with other MRI-visible PVS assessments, EPC is limited in its capacity to capture gross enlargement of white matter PVS, risking an underestimation of global PVS by excluding sub-voxel and grey matter PVS<sup>32</sup>. While we did see the high EPC volume in our untreated subjects, the absence of significant group differences in EPC-derived PVS burden after normalization, either highlights the lower sensitivity and higher variability of this approach to detect PVS differences in smaller cohorts and potentially in OSA more broadly.

In contrast, pCSF mapping (Zhou et al., 2025; Zhou et al., 2023; Zhou et al., 2024a) revealed robust group differences in parenchymal glymphatic fluid burden associated with OSA. Untreated participants showed elevated pCSF within the global ADmask (Mosconi et al., 2010) as well as across multiple lobar regions previously implicated in both sleep-related metabolic stress (Yaouhi et al., 2009; Wu et al., 2025; Li et al., 2023) and early Alzheimer's disease pathogenesis (Palmqvist et al., 2017; Serrano-Pozo et al., 2011; Teipel et al., 2020). Importantly, CPAP-treated participants, exhibited pCSF levels statistically comparable to both healthy controls and untreated subjects, potentially supporting treatment related effects on glymphatic fluid distribution. Exploratory regional analysis further revealed that elevated pCSF in untreated OSA was pronounced within basal ganglia and higher-order cortical association areas, regions known to be particularly vulnerable to cerebrovascular damage (Luigetti et al., 2012; Park, 2016; Yanagisawa, 2018; Yan et al., 2021). These results support previous findings that pCSF is more sensitive to early changes in glymphatic fluid distribution (Zhou et al., 2025), and a feasible noninvasive neuroimaging biomarker for evaluation of glymphatic fluid in OSA.

### 4.2. pCSF, amyloid burden, and sleep

In the subset of participants with available amyloid PET imaging, we did not observe significant group level differences in A $\beta$  deposition across diagnostic categories. However, across all subjects, higher pCSF within the ADmask was robustly associated with increased PiB SUVR. Specifically, elevated ADmask pCSF independently predicted greater PiB SUVR after adjustment for age and sex, and this relationship remained stable after accounting for OSA status. This association between pCSF and A $\beta$  is consistent with prior work within our group (Zhou et al., 2025; Zhou et al., 2024a), and aligns with extensive preclinical findings showing glymphatic impairment results in increased amyloid deposition (Iliff et al., 2012; Pedersen et al., 2023; Simon et al., 2022; Mestre et al., 2018a).

Importantly, while untreated OSA was associated with higher pCSF defined glymphatic fluid distribution across regions, OSA status alone did not independently explain variability in A $\beta$  burden within this cohort. Although causality cannot be inferred from this study, these cross-sectional findings suggest that sleep apnea may contribute to the accumulation of glymphatic fluid distribution, indicating of impaired glymphatic function, without directly impacting A $\beta$  deposition.

Collectively, these findings support pCSF as a neuroimaging biomarker of glymphatic fluid distribution relevant in the assessment of sleep health and neurodegenerative disease progression. Further longitudinal evaluation of glymphatic fluid distribution as a mechanistic contributor to neurodegenerative vulnerability in patients with OSA should be explored.

## 5. Limitations and future directions

While this study provides novel insight into perivascular glymphatic fluid alterations associated with OSA, several limitations should be considered. Namely, the sample size is modest, limiting the interpretation and statistical power as well as increasing susceptibility to variability arising from clinical heterogeneity inherent in OSA populations. Although regression analyses accounted for key demographic covariates, residual confounds driving neuroimaging and cognitive changes cannot be excluded. In particular, objective features of OSA severity and CPAP-treatment adherence and duration were not uniformly available. Reported use was determined through self-report and variable clinical documentation, which does not capture nightly compliance nor treatment efficacy. Our small sample size, and the absence of a significant association between pCSF and CPAP-treatment in adjusted models together underscore the need for longitudinal within-subject and adherence-verified studies to determine if CPAP driven improvement in sleep quality and oxygen saturation effect of treatment glymphatic fluid dynamics.

Additionally, while multi-echo FAST T2 enables the separation of long T2 defined pCSF across the parenchyma, this should be approached as a quantitative imaging marker of CSF-like water within MRI-visible and sub-voxel perivascular spaces rather than definitive of glymphatic function or clearance. Future validation using multi-modal neuroimaging approaches with the capacity for assessing glymphatic fluid movement (i.e. Contrast-based clearance, arterial spin labeling, diffusion tensor imaging, fMRI) will be important to further refine mechanistic specificity. We have previously defined associations between impaired sleep and tau (Kim et al., 2024b). Further longitudinal studies should determine whether changes in pCSF associated with OSA predict cognitive performance or A $\beta$  and tau accumulation. Similarly, integration of pCSF mapping with complementary neuroimaging biomarkers, such as diffusion tensor imaging and arterial spin labeling-based methods (Ford et al., 2022; Guo et al., 2025; Guo et al., 2024; Lee et al., 2024), could provide more comprehensive characterization of fluid dynamics associated with OSA.

## 6. Conclusions

In summary, this study demonstrates that untreated OSA is associated with elevated pCSF burden across multiple regions, consistent with altered glymphatic fluid distribution. These changes were not detectable using conventional MRI-visible PVS measures, underscoring the higher physiologic sensitivity of pCSF mapping for detecting subtle perivascular alterations. Importantly, CPAP-treated participants, exhibited pCSF levels comparable to healthy controls. Together, our findings support the role of glymphatic dysfunction in OSA patients and identify pCSF mapping as a promising biomarker for the clinical evaluation of glymphatic fluid distribution.

## Funding acknowledgement

This work was supported in part by the United States National Institutes of Health National Institute on Aging grants R01AG057848 and R01AG077576, the National Center for Advancing Translational Sciences of the National Institutes of Health UL1TR002384 and KL2TR002385 (SK). The content is solely the responsibility of the authors and does not necessarily represent the official views of the National Institutes of Health.

## CRediT authorship contribution statement

**Samantha A. Keil:** Writing – review & editing, Writing – original draft, Visualization, Validation, Project administration, Methodology, Investigation, Funding acquisition, Formal analysis, Data curation, Conceptualization. **Yi Li:** Writing – review & editing, Resources, Project administration, Methodology, Funding acquisition. **Ana C. Krieger:** Writing – review & editing, Supervision. **Xiuyuan H. Wang:** Writing – review & editing, Visualization, Methodology, Data curation. **Thanh D. Nguyen:** Writing – review & editing, Resources. **Jana Ivanidze:** Writing – review & editing, Supervision. **Gloria C. Chiang:** Writing – review & editing, Resources. **Tracy A. Butler:** Writing – review & editing, Supervision, Resources, Project administration. **Liangdong Zhou:** Writing – review & editing, Visualization, Validation, Supervision, Software, Project administration, Methodology, Investigation, Formal analysis, Data curation.

## Declaration of competing interest

JI receives research funding from GE Healthcare, Curium Pharma, and PI grant funding to the institution, as well as travel support from Siemens Healthineers and GEHC. GCC receives consulting fees from Life Molecular Imaging for the review of amyloid PET scans, honoraria from Efficient CME and Peerview for giving CME education lectures, and research funds from Minoryx Therapeutics.

## Appendix A. Supplementary data

Supplementary data to this article can be found online at <https://doi.org/10.1016/j.nbd.2026.107325>.

## Data availability

Raw data were generated at the Brain Health Imaging Institute (BHII) at Weill Cornell Medicine (WCM). Derived data and code for analysis supporting the findings of this study are available upon reasonable request from the corresponding authors.

## References

- Bangash, A., Wajid, F., Poolacherla, R., Mim, F.K., Rutkofsky, I.H., 2020. Obstructive sleep Apnea and hypertension: a review of the relationship and pathogenic association. *Cureus* 12, e8241. <https://doi.org/10.7759/cureus.8241>.
- Benjafield, A.V., et al., 2019. Estimation of the global prevalence and burden of obstructive sleep apnoea: a literature-based analysis. *Lancet Respir. Med.* 7, 687–698. [https://doi.org/10.1016/S2213-2600\(19\)30198-5](https://doi.org/10.1016/S2213-2600(19)30198-5).
- Benveniste, H., et al., 2017. Anesthesia with dexmedetomidine and low-dose isoflurane increases solute transport via the glymphatic pathway in rat brain when compared with high-dose isoflurane. *Anesthesiology* 127, 976–988. <https://doi.org/10.1097/ALN.0000000000001888>.
- Buysse, D.J., Reynolds 3rd, C.F., Monk, T.H., Berman, S.R., Kupfer, D.J., 1989. The Pittsburgh sleep quality index: a new instrument for psychiatric practice and research. *Psychiatry Res.* 28, 193–213. [https://doi.org/10.1016/0165-1781\(89\)90047-4](https://doi.org/10.1016/0165-1781(89)90047-4).
- Chang, J.L., et al., 2023. International consensus statement on obstructive sleep Apnea. *Int Forum Allergy Rhinol* 13, 1061–1482. <https://doi.org/10.1002/alr.23079>.
- Cui, H., et al., 2021. Decreased AQP4 expression aggravates  $\alpha$ -synuclein pathology in Parkinson's disease mice, possibly via impaired glymphatic clearance. *J. Mol. Neurosci.* 71, 2500–2513. <https://doi.org/10.1007/s12031-021-01836-4>.
- Dagum, P., et al., 2025. A wireless device for continuous measurement of brain parenchymal resistance tracks glymphatic function in humans. *Nat. Biomed. Eng.* <https://doi.org/10.1038/s41551-025-01394-9>.
- Eide, P.K., Vinje, V., Pripp, A.H., Mardal, K.A., Ringstad, G., 2021. Sleep deprivation impairs molecular clearance from the human brain. *Brain* 144, 863–874. <https://doi.org/10.1093/brain/awaa443>.
- Fischl, B., 2012. FreeSurfer. *Neuroimage* 62, 774–781. <https://doi.org/10.1016/j.neuroimage.2012.01.021>.
- Ford, J.N., et al., 2022. Quantitative water permeability mapping of blood-brain-barrier dysfunction in aging. *Front. Aging Neurosci.* 14, 867452. <https://doi.org/10.3389/fnagi.2022.867452>.
- Gribsholt, S.B., et al., 2025. Obstructive sleep apnoea and risk of dementia: a Danish population-based cohort study. *BMJ Neurol Open* 7, e001174. <https://doi.org/10.1136/bmjno-2025-001174>.

- Guo, Y., et al., 2024. Quantitative transport mapping of multi-delay arterial spin labeling MRI detects early blood perfusion alterations in Alzheimer's disease. *Alzheimer's Res Ther.* 16, 156. <https://doi.org/10.1186/s13195-024-01524-6>.
- Guo, Y., et al., 2025. Decreased quantitative transport mapping velocity in the middle cerebral artery-supplied temporal lobe in Alzheimer's disease. *Alzheimers Dement.* 21, e70540. <https://doi.org/10.1002/alz.70540>.
- Hablitz, L.M., et al., 2019. Increased glymphatic influx is correlated with high EEG delta power and low heart rate in mice under anesthesia. *Sci. Adv.* 5, eaav5447. <https://doi.org/10.1126/sciadv.aav5447>.
- Hablitz, L.M., et al., 2020. Circadian control of brain glymphatic and lymphatic fluid flow. *Nat. Commun.* 11, 4411. <https://doi.org/10.1038/s41467-020-18115-2>.
- Harrison, I.F., et al., 2020. Impaired glymphatic function and clearance of tau in an Alzheimer's disease model. *Brain* 143, 2576–2593. <https://doi.org/10.1093/brain/awaal179>.
- Holti, J.K., et al., 2019. The sleep-wake cycle regulates brain interstitial fluid tau in mice and CSF tau in humans. *Science* 363, 880–884. <https://doi.org/10.1126/science.aaa2546>.
- Iliff, J.J., et al., 2012. A paravascular pathway facilitates CSF flow through the brain parenchyma and the clearance of interstitial solutes, including amyloid  $\beta$ . *Sci. Transl. Med.* 4, 147ra111. <https://doi.org/10.1126/scitranslmed.3003748>.
- Iliff, J.J., et al., 2013. Cerebral arterial pulsation drives paravascular CSF-interstitial fluid exchange in the murine brain. *J. Neurosci.* 33, 18190–18199. <https://doi.org/10.1523/JNEUROSCI.1592-13.2013>.
- Iliff, J.J., et al., 2014. Impairment of glymphatic pathway function promotes tau pathology after traumatic brain injury. *J. Neurosci.* 34, 16180. <https://doi.org/10.1523/JNEUROSCI.3020-14.2014>.
- Ishida, K., et al., 2022. Glymphatic system clears extracellular tau and protects from tau aggregation and neurodegeneration. *J. Exp. Med.* 219. <https://doi.org/10.1084/jem.20211275>.
- Jia, Y., et al., 2021. Enlarged perivascular space and its correlation with polysomnography indicators of obstructive sleep Apnea. *Nat Sci Sleep* 13, 863–872. <https://doi.org/10.2147/NSS.S305465>.
- Jiang-Xie, L.F., et al., 2024. Neuronal dynamics direct cerebrospinal fluid perfusion and brain clearance. *Nature* 627, 157–164. <https://doi.org/10.1038/s41586-024-07108-6>.
- Kang, J.E., et al., 2009. Amyloid-beta dynamics are regulated by orexin and the sleep-wake cycle. *Science* 326, 1005–1007. <https://doi.org/10.1126/science.1180962>.
- Keil, S.A., Jansson, D., Braun, M., Iliff, J.J., 2025. Glymphatic dysfunction in Alzheimer's disease: a critical appraisal. *Science* 389, eadv8269. <https://doi.org/10.1126/science.adv8269>.
- Kim, J., Yoo, I.D., Lim, J., Moon, J.S., 2024a. Pathological phenotypes of astrocytes in Alzheimer's disease. *Exp. Mol. Med.* 56, 95–99. <https://doi.org/10.1038/s12276-023-01148-0>.
- Kim, N.H., 2012. Obstructive sleep apnea and abnormal glucose metabolism. *Diabetes Metab.* 36, 268–272. <https://doi.org/10.4093/dmj.2012.36.4.268>.
- Kim, R.T., et al., 2024b. Impaired sleep is associated with tau deposition on (18)F-floratacupir PET and accelerated cognitive decline, accounting for medications that affect sleep. *J. Neurol. Sci.* 458, 122927. <https://doi.org/10.1016/j.jns.2024.122927>.
- Kohler, M., Stradling, J.R., 2010. Mechanisms of vascular damage in obstructive sleep apnea. *Nat. Rev. Cardiol.* 7, 677–685. <https://doi.org/10.1038/nrcardio.2010.145>.
- Lan, H., et al., 2023. Weakly supervised perivascular spaces segmentation with salient guidance of Frangi filter. *Magn. Reson. Med.* 89, 2419–2431. <https://doi.org/10.1002/mrm.29593>.
- Lee, K., et al., 2024. Clinical arterial spin-Labeling MR imaging to screen for typical and atypical neurodegenerative disease in the new era of Alzheimer treatment. *AJNR Am. J. Neuroradiol.* 45, 632–636. <https://doi.org/10.3174/ajnr.A8164>.
- Li, J., S. T., Huang, Y., Mettenburg, J.M., Ibrahim, T.S., Aizenstein, H.J., Wu, M., 2024. Wmh\_seg: transformer based U-Net for robust and automatic white matter hyperintensity segmentation across 1.5T, 3T and 7T. arxiv:2402.12701 1–12.
- Li, X., et al., 2023. Altered cerebral blood flow and white matter during wakeful rest in patients with obstructive sleep apnea: a population-based retrospective study. *Br. J. Radiol.* 96, 20220867. <https://doi.org/10.1259/bjr.20220867>.
- Lin, S., et al., 2024. Association of MRI indexes of the perivascular space network and cognitive impairment in patients with obstructive sleep Apnea. *Radiology* 311, e232274. <https://doi.org/10.1148/radiol.232274>.
- Lopes, D.M., et al., 2025. The influence of the glymphatic system on alpha-synuclein propagation: the role of aquaporin-4. *Brain*. <https://doi.org/10.1093/brain/awaf255>.
- Lord, A.R., Amitrano, N.R., Gonzalez, D.A., 2024. Reliability and validity of the Montreal cognitive assessment's auditory items (MoCA-22). *Clin. Neuropsychol.* 38, 783–798. <https://doi.org/10.1080/13854046.2023.2261634>.
- Luigetti, M., Goldsberry, G.T., Cianfoni, A., 2012. Brain MRI in global hypoxia-ischemia: a map of selective vulnerability. *Acta Neurol. Belg.* 112, 105–107. <https://doi.org/10.1007/s13760-012-0007-3>.
- Mestre, H., et al., 2018a. Aquaporin-4-dependent glymphatic solute transport in the rodent brain. *Elife* 7. <https://doi.org/10.7554/elife.40070>.
- Mestre, H., et al., 2018b. Flow of cerebrospinal fluid is driven by arterial pulsations and is reduced in hypertension. *Nat. Commun.* 9, 4878. <https://doi.org/10.1038/s41467-018-07318-3>.
- Morris, J.C., 1997. Clinical dementia rating: a reliable and valid diagnostic and staging measure for dementia of the Alzheimer type. *Int. Psychogeriatr.* 9 Suppl 1, 173–176 discussion 177–178. <https://doi.org/10.1017/s1041610297004870>.
- Mosconi, L., et al., 2010. Increased fibrillar amyloid-beta burden in normal individuals with a family history of late-onset Alzheimer's. *Proc. Natl. Acad. Sci. USA* 107, 5949–5954. <https://doi.org/10.1073/pnas.0914141107>.
- Nguyen, T.D., et al., 2016. Feasibility and reproducibility of whole brain myelin water mapping in 4 minutes using fast acquisition with spiral trajectory and adiabatic T2prep (FAST-T2) at 3T. *Magn. Reson. Med.* 76, 456–465. <https://doi.org/10.1002/mrm.25877>.
- Palmqvist, S., et al., 2017. <article-title update="modified" original="Earliest accumulation of beta-amyloid occurs within the default-mode network and concurrently affects brain connectivity">Earliest accumulation of  $\beta$ -amyloid occurs within the default-mode network and concurrently affects brain connectivity. *Nat. Commun.* 8, 1214. <https://doi.org/10.1038/s41467-017-01150-x>.
- Park, J., 2016. Movement disorders following cerebrovascular lesion in the basal ganglia circuit. *J Mov Disord* 9, 71–79. <https://doi.org/10.14802/jmd.16005>.
- Pedersen, T.J., Keil, S.A., Han, W., Wang, M.X., Iliff, J.J., 2023. The effect of aquaporin-4 mis-localization on Abeta deposition in mice. *Neurobiol. Dis.* 181, 106100. <https://doi.org/10.1016/j.nbd.2023.106100>.
- Sepehrband, F., et al., 2019. Image processing approaches to enhance perivascular space visibility and quantification using MRI. *Sci. Rep.* 9, 12351. <https://doi.org/10.1038/s41598-019-48910-x>.
- Serrano-Pozo, A., Frosch, M.P., Masliah, E., Hyman, B.T., 2011. Neuropathological alterations in Alzheimer disease. *Cold Spring Harb. Perspect. Med.* 1, a006189. <https://doi.org/10.1101/cshperspect.a006189>.
- Simon, M., et al., 2022. Loss of perivascular aquaporin-4 localization impairs glymphatic exchange and promotes amyloid  $\beta$  plaque formation in mice. *Alzheimer's Res. Ther.* 14, 59. <https://doi.org/10.1186/s13195-022-00999-5>.
- Slowik, J.M., Sankari, A., Collen, J.F., 2025. StatPearls.
- Teipel, S.J., et al., 2020. In vivo staging of regional amyloid deposition predicts functional conversion in the preclinical and prodromal phases of Alzheimer's disease. *Neurobiol. Aging* 93, 98–108. <https://doi.org/10.1016/j.neurobiolaging.2020.03.011>.
- Ungvari, Z., et al., 2025. Sleep disorders increase the risk of dementia, Alzheimer's disease, and cognitive decline: a meta-analysis. *Geroscience* 47, 4899–4920. <https://doi.org/10.1007/s11357-025-01637-2>.
- van Veluut, S.J., et al., 2020. Vasomotion as a driving force for paravascular clearance in the awake mouse brain. *Neuron* 105, 549–561.e545. <https://doi.org/10.1016/j.neuron.2019.10.033>.
- Villemagne, V.L., et al., 2013. Amyloid beta deposition, neurodegeneration, and cognitive decline in sporadic Alzheimer's disease: a prospective cohort study. *Lancet Neurol.* 12, 357–367. [https://doi.org/10.1016/S1474-4422\(13\)70044-9](https://doi.org/10.1016/S1474-4422(13)70044-9).
- Wang, J., et al., 2023. Impaired glymphatic drainage underlying obstructive sleep apnea is associated with cognitive dysfunction. *J. Neurol.* 270, 2204–2216. <https://doi.org/10.1007/s00415-022-11530-z>.
- Wu, K., et al., 2025. Obstructive sleep apnea and structural and functional brain alterations: a brain-wide investigation from clinical association to genetic causality. *BMC Med.* 23, 42. <https://doi.org/10.1186/s12916-025-03876-8>.
- Xie, L., et al., 2013. Sleep drives metabolite clearance from the adult brain. *Science* 342, 373–377. <https://doi.org/10.1126/science.1241224>.
- Xu, Z., et al., 2015. Deletion of aquaporin-4 in APP/PS1 mice exacerbates brain  $\alpha\beta$  accumulation and memory deficits. *Mol. Neurodegener.* 10, 58. <https://doi.org/10.1186/s13024-015-0056-1>.
- Yan, L., et al., 2021. Altered regional cerebral blood flow in obstructive sleep apnea is associated with sleep fragmentation and oxygen desaturation. *J. Cereb. Blood Flow Metab.* 41, 2712–2724. <https://doi.org/10.1177/0271678X21102109>.
- Yanagisawa, N., 2018. Functions and dysfunctions of the basal ganglia in humans. *Proc. Jpn. Acad. Ser. B Phys. Biol. Sci.* 94, 275–304. <https://doi.org/10.2183/pjab.94.019>.
- Yaouhi, K., et al., 2009. A combined neuropsychological and brain imaging study of obstructive sleep apnea. *J. Sleep Res.* 18, 36–48. <https://doi.org/10.1111/j.1365-2869.2008.00705.x>.
- Zhou, L., et al., 2023. Association of brain tissue cerebrospinal fluid fraction with age in healthy cognitively normal adults. *Front. Aging Neurosci.* 15, 1162001. <https://doi.org/10.3389/fnagi.2023.1162001>.
- Zhou, L., et al., 2024a. Parenchymal CSF fraction is a measure of brain glymphatic clearance and positively associated with amyloid beta deposition on PET. *Alzheimers Dement.* 20, 2047–2057. <https://doi.org/10.1002/alz.13659>.
- Zhou, L., et al., 2024b. Multimodal assessment of brain fluid clearance is associated with amyloid-beta deposition in humans. *J. Neuroradiol.* 51, 101164. <https://doi.org/10.1016/j.neurad.2023.10.009>.
- Zhou, L., et al., 2025. Brain glymphatic fluid mapping in Alzheimer's disease: a human MRI and PET study. *Brain Commun.* 7, fcaf200. <https://doi.org/10.1093/braincomms/fcaf200>.